Role of Resonances on Microwave Heating of Oil–Water Emulsions

Tanmay Basak
Dept. of Chemical Engineering, Indian Institute of Technology, Madras, Chennai 600 036, India

DOI 10.1002/aic.10207
Published online in Wiley InterScience (www.interscience.wiley.com).

A detailed analysis on enhanced heating effects attributed to resonance of microwaves has been carried out to study the efficient heating methodologies for oil–water emulsions. Studies on heating have been carried out for samples incident with microwaves at one side and at both sides. The maxima in average power corresponding to resonances occur at various sample thicknesses for all emulsions and we consider two dominant resonance modes R_1 *and* R_2*, where the average power at* R_1 *is larger than that at* R_2*. During one side incidence, it is observed that processing rates are greater at the* R_2 *mode for both oil-in-water (o/w) and water-in-oil (w/o) emulsions, whereas for both-sides incidence, the* R_1 *mode is favored for o/w emulsion and the* R_2 *mode is advantageous for w/o emulsion. The greater rates in thermal processing are observed when the emulsions (o/w and w/o) are incident at both sides. Current analysis recommends on the efficient way to use microwaves in a customized plane-wave oven for greater heating effects and determines the optimal sample thicknesses vs. various oil–water contents for thermal processing. The emulsion system is a combination of materials with very low dielectric loss (oil) and high dielectric loss (water), and the effective dielectric response is highly nontrivial to predict the efficient way to heat an emulsion, either o/w or w/o.* © 2004 American Institute of Chemical Engineers *AIChE J,* 50: 2659–2675, 2004
Keywords: microwave, resonances, oil–water emulsion

Introduction

Microwave (MW) energy has been widely applied in food and chemical processing for heating, thawing, sintering of ceramics, and many others (Ayappa et al., 1992; Basak and Ayappa, 1997, 2001; Chatterjee et al., 1998; Ratanadecho et al., 2002). Various oil-in-water (o/w) and water-in-oil (w/o) emulsions occur in industrial operations, such as petroleum refining, oil and gas production, and food processing industries, which include dressings, sauces, butter, mayonnaise, and many more. Efficient heating of emulsions is required for a faster processing based on industrial demand. Microwave heating, because of its volumetric heating effects, offers a faster processing rate. The enhanced processing can be achieved by heating samples in the presence of resonances, which occur as the result of constructive interference of propagating waves within a material for specific sample dimensions, corresponding to a relationship between sample dimensions, wavelength, and penetration depths, whereas resonances are absent for a very large or very small dimension (Ayappa et al., 1997).

A few earlier investigations on resonances were carried out for cylinders and spheres (Massoudi et al., 1979; Ohlsson and Risman, 1978; Weil, 1975). Ohlsson and Risman (1978) carried out experimental studies on MW heating at 2450 MHz for spherical and cylindrical samples and they observed resonances in power absorption at the center of the sample for specific radii. Massoudi et al. (1979) observed resonances for multilayered samples while studying average power absorption in homogeneous and multilayered cylinders by varying the frequency of radiation. Weil (1975) studied average power over the frequency range for spheres of radii 3.3 and 6 cm, where strong resonances were observed when the frequency was varied.

Correspondence concerning this article should be addressed to T. Basak at tanmay@iitm.ac.in.

A number of theoretical and numerical analysis of resonances of power due to MW heating in slabs and cylinders for uniform plane waves were also carried out by earlier investigators (Ayappa et al., 1997; Barringer et al., 1994; Basak, 2003). The theoretical predictions are obtained from an energy balance equation, where the volumetric heat generation is obtained from solving Maxwell's equation. Barringer et al. (1994) found that the resonating effect is more pronounced in water than in oil samples. Ayappa et al. (1997) and Ayappa (1999) analyzed resonances in slabs and cylinders for various materials. Basak (2003) analyzed resonances for multiphase samples with the individual role of transmitted and reflected waves within a sample while investigating the MW thawing process.

A number of studies were carried out on MW heating of oil and water systems where resonances were also reported for specific cases. Microwave heating of oil and water samples shows that, with decreasing sample size, the heating rate of water samples increases much faster than that of oil sample (Barringer et al., 1994). For small samples, the MW power absorption in water shows oscillatory behavior with the sample size, whereas the oil samples result in size-invariant low MW power absorption. The greater dielectric loss of water seems to play a critical role in developing internal reflections, to produce an oscillatory behavior of power. The MW heating of small size samples with uniform plane wave shows features identical to those seen in a customized oven (Barringer et al., 1994). Some earlier studies (Fu and Metaxes, 1992; Pescheck et al., 1992) also reported that MW heating of smaller size samples shows strong oscillatory behavior.

A detailed experimental investigation on MW heating of oil–water emulsion systems was carried out by Barringer et al. (1995). They carried out experimental studies for various oil–water fractions with fixed beaker radii in a microwave oven. They observed a maximum heating rate for 20 and 40% water in o/w emulsion systems as the beaker radius was fixed. Their experimental data were further validated with some ad hoc theoretical model and a similar qualitative trend was observed. As the beaker size was fixed, they observed resonances corresponding to higher heating rates for certain combinations of beaker radius and dielectric properties. They also studied the heating rates for w/o emulsions and it is found that the w/o emulsions heat at 43% of the rate of the o/w emulsion of the same concentration. Fang and Lai (1995) and Chen and Chan (2002) carried out experimental studies, especially on w/o emulsions, while they investigated the conditions of deemulsification of w/o emulsions, which is important in the application of emulsion liquid membrane in separation processes.

Although earlier experimental studies were carried out to investigate various heating characteristics of o/w and w/o emulsions, there is a conspicuous absence of efficient heating strategy of emulsions where resonances may play a critical role in faster processing. Motivated by the work of Barringer et al. (1995), we attempt to establish in this report a detailed theoretical understanding on resonance for any o/w or w/o emulsions, by varying the sample size, and to recommend an efficient heating strategy. The results would be the potential guideline on the efficient use of microwaves for enhanced heating of oil–water emulsion systems where the heating attributed to microwaves is highly nontrivial because of the complex dielectric response.

Here we carry out a detailed analysis of resonances during MW heating of o/w and w/o samples. Our analysis is illustrated for one-dimensional (1-D) slabs incident with uniform plane waves. MW propagation within a sample is governed by Maxwell's equations whose solution is a linear combination of the traveling waves ascribed to transmission and reflection. An analytical solution has been developed to study the influence of traveling waves on MW power distributions for a multicomponent system. The power absorption in the emulsion system depends largely on whether the continuous phase is oil or water and we modeled the effective dielectric response in oil–water emulsions, based on a recent study (Erle et al., 2000) that illustrates that dielectric response in o/w systems is quite different from that in w/o systems for similar oil–water ratios. Although the size of dispersed phases, oil or water, critically alters the internal reflections within an emulsion sample, we restrict our current studies with the droplet sizes of dispersed phases between 5 and 15 μm as the deemulsification, particularly for w/o sample decreases with the smaller sizes of droplets (see Erle et al., 2000).

The resonances in MW power are illustrated with the average power vs. sample thicknesses. The primary and secondary modes of resonances, which are functions of sample thicknesses, are identified to investigate the influence of resonances. Note that the average power is smaller in the secondary mode, which corresponds to a larger processing length than that in the primary mode. Microwave heating is modeled with an energy balance equation in which heat generation attributed to MW power is a function of electric fields. Heating characteristics have been contrasted for 50% o/w and 50% w/o samples during primary and secondary resonance modes. The heating with one-side incidence is contrasted with both-sides incidence and for all cases, based on greater material processing rates, the processing lengths are determined for various fractions of oil–water emulsions. Recommendations are made as to whether both-sides incidence or one-side incidence is advantageous for various o/w and w/o emulsions.

Theory

Distribution of electric fields and phase states in a multilayered slab

The wave propagation attributed to a uniform electric field E_x within a medium is governed by (Ayappa et al., 1991)

$$\frac{d^2E_x}{dz^2} + k^2E_x = 0 \tag{1}$$

where E_x lies in the x–y plane and varies only along the direction of propagation, z-axis (Figure 1) and the propagation constant

$$k = \frac{\omega}{c}\sqrt{\kappa' + i\kappa''} \tag{2}$$

depends on the dielectric constant κ' and the dielectric loss κ''. Here $\omega = 2\pi f$, where f is the frequency of the electromagnetic wave and c is the velocity of light. The 1D slab is surrounded by the air medium and the electric field distribution for the lth medium in a composite obtained from Eq. 1 is

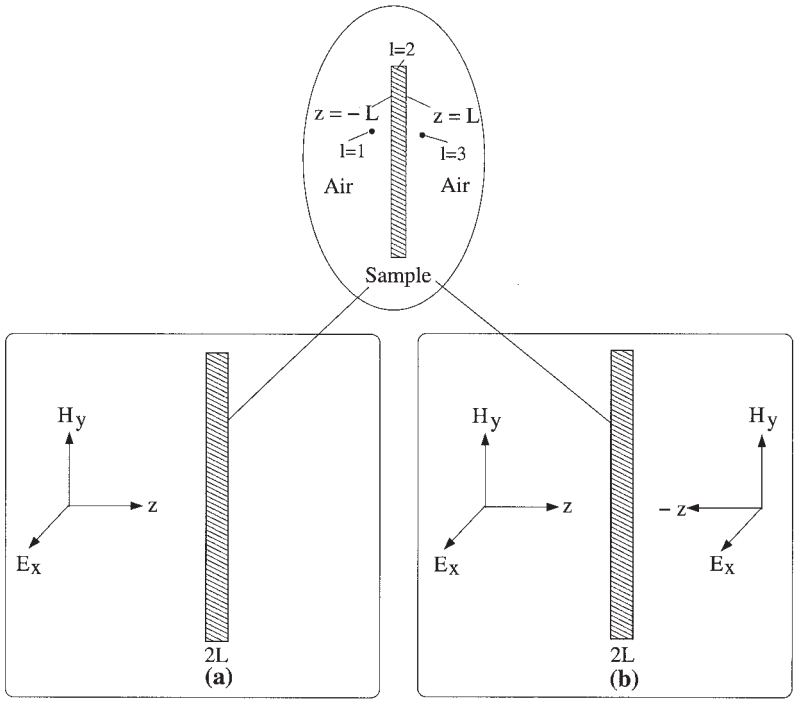

Figure 1. 1-D slab exposed to a plane electromagnetic wave with (a) one-side incidence and (b) both-sides incidences.

A multilayered sample is typically characterized by air–sample–air layers.

$$\frac{d^2E_{x,l}}{dz^2} + k_l^2 E_{x,l} = 0 \tag{3}$$

where $z_{l-1} \le z \le z_l$ and $l = 1$–3. Note that, $l = 1, 3$ denotes air medium and $l = 2$ denotes the sample as seen in Figure 1. We assume each layer has constant dielectric properties and, thus, the general solution to Eq. 3, represented as a linear combination of traveling waves propagating in opposite directions, is

$$E_{x,1} = E_{t,1}e^{ik_1z} + E_{r,1}e^{-ik_1z} \qquad z \le z_1$$

$$E_{x,2} = E_{t,2}e^{ik_2z} + E_{r,2}e^{-ik_2z} \qquad z_1 \le z \le z_2$$

$$E_{x,3} = E_{t,3}e^{ik_3z} + E_{r,3}e^{-ik_3z} \qquad z \ge z_2 \tag{4}$$

where $E_{t,l}$ and $E_{r,l}$ are the coefficients attributed to transmission and reflection, respectively. The boundary conditions at the interface are

$$\left.\begin{aligned} E_{x,l-1} &= E_{x,l} \\ \frac{dE_{x,l-1}}{dz} &= \frac{dE_{x,l}}{dz} \end{aligned}\right\} \qquad \begin{aligned} l &= 2, 3 \\ z &= z_1, z_2 \end{aligned} \tag{5}$$

Using the interface conditions (Eqs. 5) and the general solutions (Eqs. 4), the coefficients $E_{t,l}$ and $E_{r,l}$ are obtained by solving the following set of algebraic equations

$$\left.\begin{aligned} E_{t,l}e^{ik_lz_l} + E_{r,l}e^{-ik_lz_l} - E_{t,l+1}e^{ik_{l+1}z_l} - E_{r,l+1}e^{-ik_{l+1}z_l} &= 0 \\ k_lE_{t,l}e^{ik_lz_l} - k_lE_{r,l}e^{-ik_lz_l} - k_{l+1}E_{t,l+1}e^{ik_{l+1}z_l} + k_{l+1}E_{r,l+1}e^{-ik_{l+1}z_l} &= 0 \end{aligned}\right\} \qquad l = 1, 2 \tag{6}$$

Because the incident field intensities from the left and right surfaces are known (that is, $E_{t,1} = E_L$ and $E_{r,3} = E_R$), Eqs. 6 are solved for the remaining coefficients, following the manner similar to that discussed by Basak (2003). For the lth layer, the transmitted and reflected waves are

$$E^t_{x,l} = E_{t,l}e^{ik_lz} = A^t_{x,l}e^{i\delta^t_{x,l}}$$

$$E^r_{x,l} = E_{r,l}e^{-ik_lz} = A^r_{x,l}e^{i\delta^r_{x,l}} \tag{7}$$

where corresponding amplitudes

$$A^t_{x,l} = \sqrt{E^t_{x,l}E^{t*}_{x,l}}$$

$$A^r_{x,l} = \sqrt{E^r_{x,l}E^{r*}_{x,l}} \tag{8}$$

and the phase states

$$\delta^t_{x,l} = \tan^{-1}\left[\frac{\mathrm{Im}(E^t_{x,l})}{\mathrm{Re}(E^t_{x,l})}\right]$$

$$\delta^r_{x,l} = \tan^{-1}\left[\frac{\mathrm{Im}(E^r_{x,l})}{\mathrm{Re}(E^r_{x,l})}\right] \tag{9}$$

where the superscript * in Eq. 8 denotes the complex conjugate. For a stationary wave in the lth layer, the amplitude is

$$A_{x,l} = \sqrt{E_{x,l}E^*_{x,l}} \tag{10}$$

and the difference in phase angle

$$\delta_{x,l} = \delta^t_{x,l} - \delta^r_{x,l} \tag{11}$$

where the quantities $E_{x,l}$ and $E^*_{x,l}$ appeared in Eq. 10, are evaluated using Eqs. 4 and 7. At the resonance, the difference in phase angle is zero, that is, $\delta_{x,l} = 0$.

The overall analysis of amplitudes and phase states of electric fields needs special mention. For the first and third media, $E_{t,1} = E_L$ and $E_{r,3} = E_R$, where E_L and E_R are incident electric field intensities on the left and right surfaces, respectively. The incident field intensities E_L and E_R can be evaluated using Eq. 13 as given later. The electric fields $E^t_{x,1}$ and $E^r_{x,3}$ can be expressed in terms of amplitudes and phase states, as given in Eq. 7. Therefore, the amplitudes and phase states of the incident waves on each surface are determined uniquely. For the first medium, $E^t_{x,1} = A^t_{x,1}e^{i\delta^t_{x,l}}$, where the amplitude, $A^t_{x,1} = E_L$ and phase states of the incident wave on the left surface can be calculated based on dielectric properties in free space. Note that the resultant electric field in the first medium is $E_{x,1} \neq E_{t,1}e^{ik_1 z}$ and the boundary conditions at the air–surface interface are obtained with the continuity on functions and derivatives of the resultant electric field (see Eq. 5).

The power for lth layer, obtained from the Poynting vector theorem, is

$$q(z) = \frac{1}{2}\omega\varepsilon_0\kappa'' E_{x,l}(z)\,E^*_{x,l}(z) \tag{12}$$

where ε_0 is the free space permittivity. The dielectric loss κ'' is, in general, a constant within a sample, and for various emulsions, dielectric properties may be obtained from a suitable model as discussed in the next section. For a given flux of incident radiation I_0, in free space the incident electric field intensity E_0 is given by

$$E_0 = \sqrt{\frac{2I_0}{c\varepsilon_0}} \tag{13}$$

The average power obtained by integrating the power across the slab is

$$q_{av} = \frac{1}{2L}\int_{-L}^{L} q(z)dz \approx \frac{1}{2L}\sum_{0}^{2L} q(z) \tag{14}$$

Here, $2L$ denotes the sample thickness as shown in Figure 1. We will refer to sample thickness as "processing length" for samples with various oil–water fractions.

The penetration depth D_p and wavelength of radiation in the medium λ_m are related to κ' and κ'' in the following manner

$$D_p = \frac{c}{\sqrt{2}\,\pi f\left[\kappa'\left(\sqrt{1+\left(\frac{\kappa''}{\kappa'}\right)^2}-1\right)\right]^{1/2}} \tag{15}$$

and

$$\lambda_m = \frac{c\sqrt{2}}{f\left[\kappa'\left(\sqrt{1+\left(\frac{\kappa''}{\kappa'}\right)^2}+1\right)\right]^{1/2}} \tag{16}$$

The propagation constant in Eq. 1 is

$$k = (2\pi/\lambda_m) + i(1/D_p) \tag{17}$$

The above form of propagation constant indicates that, for a fixed incident frequency and intensity, λ_m and D_p are the two length scales that determine the electric field distribution within the sample. The generalized length scales for propagation of MWs within a multiphase sample are functions of effective dielectric properties. The effective dielectric properties are strongly dependent on the nature of continuous medium, as discussed in the next section. The material dielectric loss κ'' in terms of D_p and λ_m, obtained from Eqs. 2 and 17 by equating the real and imaginary parts, is

$$\kappa'' = \frac{4\pi c^2}{\omega^2\lambda_m D_p} \tag{18}$$

Using Eqs. 13 and 18, the microwave power term in Eq. 12 is

$$q(z) = N_w N_p\left(\frac{\lambda_0\varepsilon_0 c}{4L^2}\right)E_{x,l}(z)\,E^*_{x,l}(z) \tag{19}$$

where λ_0 is the wavelength is free space, the wave number

$$N_w = \frac{2L}{\lambda_m} \tag{20}$$

and the penetration number

$$N_p = \frac{2L}{D_p} \tag{21}$$

Therefore the average power in Eq. 14

$$q_{av} = f(N_w, N_p) \tag{22}$$

which is material invariant. The detailed material invariant analysis of power distribution may be a subject for future studies.

Modeling of microwave heating in multiphase system

In this section, we have analyzed microwave heating of 1-D slabs of oil–water emulsions. The heat transport within the emulsion is governed by a single energy balance equation, assuming a local thermal equilibrium between oil and water phases. The system of o/w or w/o emulsions can be viewed as the combination of dispersed and continuous phases. The single energy balance equation within the multiphase system is

$$C_{eff}\frac{\partial T}{\partial t} = k_{eff}\frac{\partial^2 T}{\partial z^2} + q(z) \tag{23}$$

where $C_{eff} = \phi\rho C_d + (1 - \phi)\rho C_c$ is the effective heat capacity, with C_d and C_c as specific heat capacities of dispersed and continuous phases, respectively; ϕ is the volume fraction of the dispersed phase; ρ is the mean density between the dispersed and continuous phases; and $k_{eff} = \phi k_d + (1 - \phi)k_c$ is the effective thermal conductivity, with k_d and k_c as thermal conductivities of dispersed and continuous phases, respectively. In Eq. 23, $q(z)$, also defined in Eq. 12, is the absorbed microwave power. We assume a homogeneous emulsion system and the wave propagation equation for the entire domain obtained from Eq. 1 is

$$\frac{d^2E_x}{dz^2} + k^2(\phi)\,E_x = 0 \tag{24}$$

where $k = (\omega/c)\sqrt{\kappa'(\phi) + i\kappa''(\phi)}$ is the propagation constant. Erle et al. (2000) measured dielectric properties for various emulsions and they found that the effective dielectric properties for an oil–water emulsion are dependent on the nature of the continuous medium. Their experiments were carried out with mean droplet diameters varying between 5 and 15 μm, where droplet diameters were measured in a laser diffraction system. Lauryl ethylene oxide 10 and Triodan R 90 were used for stabilizing o/w and w/o emulsions, respectively. Based on their experimental studies, the effective dielectric properties for o/w emulsion given by Fricke (1955) are

$$\kappa^* = \kappa_c^*\frac{\kappa_d^*(1 + a\phi) + \kappa_c^* a(1 - \phi)}{\kappa_c^*(a + \phi) + \kappa_d^*(1 - \phi)} \tag{25}$$

where κ_c^* and κ_d^* are the relative complex dielectric properties of the continuous and dispersed phases, respectively; $a = 2$ for spherical dispersions; and $a = 1$ for cylindrical dispersions. Based on the experimental observation, $a = 1$ is chosen for dielectric properties of o/w emulsions. Experimental data on the dielectric properties of w/o emulsion were best fitted by Lichtenecker and Rother (1931) and dielectric properties are obtained as

$$\ln \kappa^* = \phi \ln \kappa_d^* + (1 - \phi)\ln \kappa_c^* \tag{26}$$

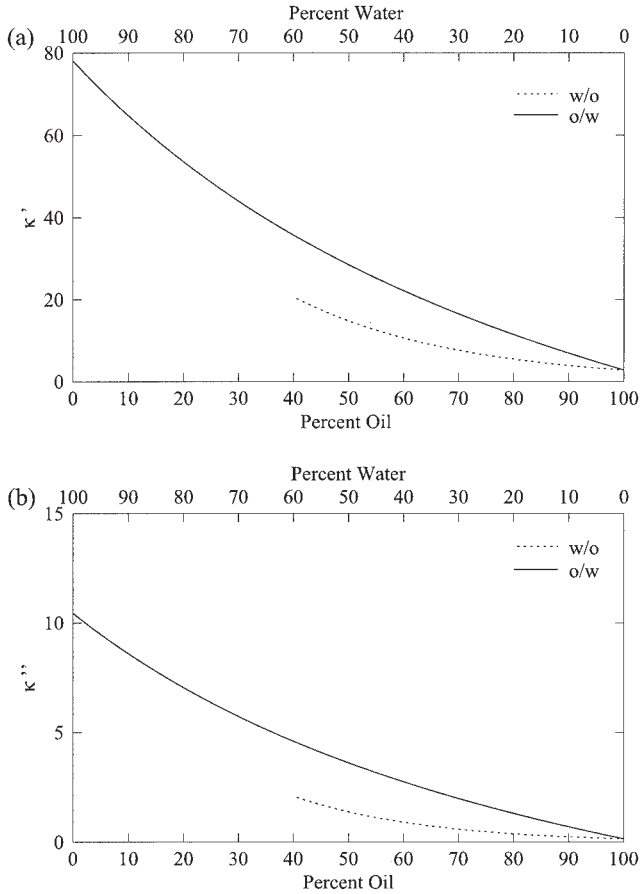

Figure 2. (a) Relative dielectric constant (κ') and (b) relative dielectric loss (κ'') for o/w and w/o emulsions.

The effective dielectric properties for o/w and w/o emulsions were obtained from Erle et al. (2000) (see Eqs. 25 and 26).

Figure 2 represents the effective dielectric properties for o/w and w/o emulsions. The dielectric properties (κ' and κ'') for o/w emulsions are greater than those for w/o emulsions. Given that water has greater dielectric properties, the effective dielectric properties for the o/w sample differ considerably from those for w/o emulsions, for identical volumetric proportions of oil and water in emulsions. Specially, for emulsions, the dielectric properties for a medium are strongly dependent on the specific component that forms the continuous medium. Enhanced dielectric properties for o/w emulsions were also reported by Barringer et al. (1995).

Dimensionless analysis and solution strategy

The electric field and energy balance equations may be solved using dimensionless variables. The dimensionless variables for electric field equations are

$$u = \frac{E_x}{E_0} \qquad \text{and} \qquad \frac{d}{dz'} \equiv 2L\frac{d}{dz}$$

Equation 24 reduces to

Table 1. Thermal and Dielectric Properties of Oil and Water

Material Property	Oil	Water
Heat capacity, C_p [W s kg^{-1} °C^{-1}]	2000	4190
Thermal conductivity, k [W m^{-1} °C^{-1}]	0.168	0.609
Density, ρ [kg m^{-3}]	900	1000
Dielectric constant (2450 MHz), κ'	2.80	78.10
Dielectric loss (2450 MHz), κ''	0.15	10.44

$$\frac{d^2u}{dz'^2} + \gamma^2(\phi)u = 0 \tag{27}$$

where u is the electric field intensity, $\gamma(\phi) = (2L\omega/c)\sqrt{\kappa'(\phi) + i\kappa''(\phi)}$ is the propagation constant and $2L$ is the thickness of the slab as shown in Figure 1. Substituting the complex field variable $u = v + iw$ into Eq. 27 and equating the real and imaginary components, we obtain

$$\frac{d^2v}{dz'^2} + \chi_1(\phi)v - \chi_2(\phi)w = 0 \tag{28}$$

and

$$\frac{d^2w}{dz'^2} + \chi_2(\phi)v + \chi_1(\phi)w = 0 \tag{29}$$

with

$$\chi_1(\phi) = \frac{4L^2\omega^2}{c^2}\kappa'(\phi) \qquad \text{and} \qquad \chi_2(\phi) = \frac{4L^2\omega^2}{c^2}\kappa''(\phi)$$

For uniform plane waves incident on a sample some of the radiation is scattered and the rest is absorbed. For a 1D slab, boundary conditions for the real and imaginary components are (Basak and Ayappa, 1997)

$$\left.\begin{aligned} \frac{dv}{dz'} - \frac{2\omega L}{c}w &= \frac{4\omega L}{c}\sin\left(\frac{\omega L}{c}\right) \\ \frac{dw}{dz'} + \frac{2\omega L}{c}v &= \frac{4\omega L}{c}\cos\left(\frac{\omega L}{c}\right) \end{aligned}\right\} \quad \text{at } z' = 0 \tag{30}$$

and

$$\left.\begin{aligned} \frac{dv}{dz'} + \frac{2\omega L}{c}w &= -\frac{E_R}{E_L}\frac{4\omega L}{c}\sin\left(\frac{\omega L}{c}\right) \\ \frac{dw}{dz'} - \frac{2\omega L}{c}v &= -\frac{E_R}{E_L}\frac{4\omega L}{c}\cos\left(\frac{\omega L}{c}\right) \end{aligned}\right\} \quad \text{at } z' = 1 \tag{31}$$

The dimensionless form of the energy balance equation in the presence of microwave, Eq. 23, is

$$\bar{C}_{eff}\frac{\partial\theta}{\partial\tau} = \bar{k}_{eff}\frac{\partial^2\theta}{\partial z'^2} + Q(\phi) \tag{32}$$

where the expression for the microwave power term in Eq. 32 is

$$Q(\phi) = \frac{2L^2\omega\varepsilon_0\kappa''(\phi)E_0^2}{k_0T_0}(v^2 + w^2) \tag{33}$$

The initial condition used in the analysis is

$$\theta(\tau = 0) = \frac{T_0 - T_\infty}{T_0} \qquad \text{for } 0 \le z' \le 1 \tag{34}$$

In the analysis, Neumann convective boundary condition is used, which can be expressed as

$$-\mathbf{n}\cdot\bar{k}_{eff}\frac{\partial\theta}{\partial z'} = Bi\theta \tag{35}$$

The electric field equation, Eq. 27, can be solved independently using the combination of traveling waves. The energy balance equation is a function of electric field distributions by the nonlinear MW power term. Alternatively, the entire system of energy balance and the electric field equations may be solved using the Galerkin finite-element method, which is suitable for solving the entire system of equations when the analytical expression on the electric field is difficult to obtain for multilayered samples or the electric field equations may be coupled with the energy balance equation by temperature-dependent dielectric properties (Basak, 2003; Basak and Ayappa, 1997, 2001).

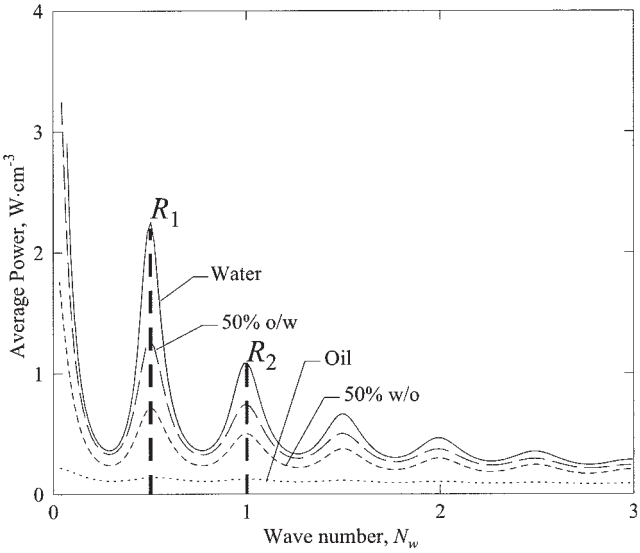

Figure 3. Average power (W cm^{-3}) vs. wave number (N_w) for water, oil, 50% o/w, and 50% w/o slabs exposed to microwaves at one side.

f = 2450 MHz; the incident MW intensity at left face, I_{OL} = 3 W cm^{-2}; the incident MW intensity at right face, I_{OR} = 0. The primary maximum in average power occurs at N_w = 0.5, corresponding to R_1 resonance mode, whereas a secondary resonance mode R_2 occurs at N_w = 1, irrespective of any materials.

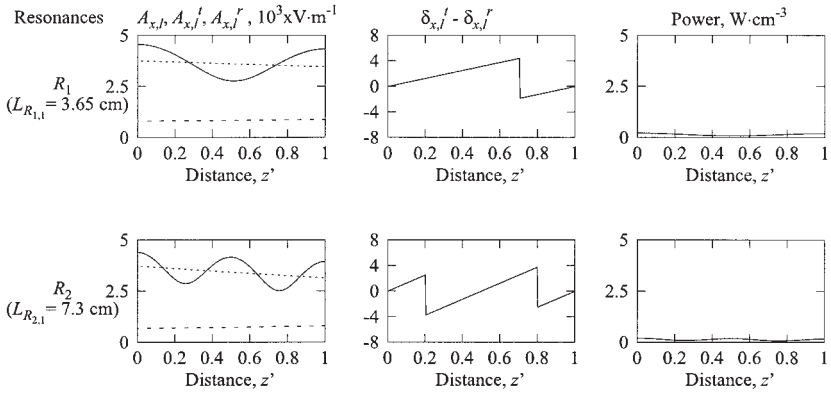

Figure 4. Amplitudes of electric field ($A_{x,l}$, $A_{x,l}^t$, $A_{x,l}^r$), phase difference ($\delta_{x,l}^t - \delta_{x,l}^r$), and power distributions for pure oil slabs exposed to microwaves from the left face.

f = 2450 MHz, I_{OL} = 3 W cm^{-2}, I_{OR} = 0. · · · , transmitted wave; – – – , reflected wave; — , stationary wave. Spatial resonances in electric fields occur at both faces for R_1 mode whereas resonances are at both faces as well as center for R_2 mode. Because of lower dielectric loss, power absorption is small throughout the sample for both resonance modes.

Results and Discussion

One-side incidence

A set of case studies has been carried out to analyze MW power characteristics and resonances for oil, water, and oil–water emulsions of 1-D slabs with one side exposed to MWs. The dielectric properties are obtained from Table 1. In all cases, the sample is exposed to the MW radiation of intensity 3 W cm^{-2}.

The influence of resonances may be illustrated by average power distribution as a function of wave number, N_w (see Eq. 22). The average power obtained from Eq. 14 is plotted as a function of N_w, as shown in Figure 3, where the maximum in average power occurs at $N_w = 0.5n$ with $n = 1, 2, \ldots$, irrespective of material, as discussed in an earlier work (Ayappa et al., 1997). We will consider two resonance modes (R_1 and R_2) occurring at $N_w = 0.5$ and 1, where the intensity of resonances decreases with larger N_w. The average power distributions for water, oil, 50% o/w, and 50% w/o samples show that, for a fixed resonance mode (R_1 or R_2), the maximum in absorbed power occurs for water, whereas the minimum corresponds to oil. Intensity of resonances also depends on the nature of the continuous medium because 50% o/w absorbs greater power than 50% w/o. These interesting features, as seen in average power vs. wave number diagram, thus provide a stimulus for determining the efficient heating route of oil–water emulsions due to MWs incidence. We will contrast the heating strategies and power distributions for the R_1 and R_2 modes. For specific materials, R_2 corresponding to $N_w = 1$ offers a greater sample thickness to be processed and our analysis will provide guidelines to choose the optimal sample thickness based on greater power absorption for a fixed microwave incidence.

During heating of oil–water emulsions, the power distributions within a sample depend on transmitted and reflected power within the medium. In reality, the scattering effects of oil drops in water are nonidentical with a medium consisting of water drops within an oil medium. Detailed analysis are beyond the scope of the current work. Here we present the analysis of microwave propagations for oil, water, and oil–water emulsions (o/w and w/o) at resonances R_1 and R_2.

The maxima in spatial power absorption of the stationary

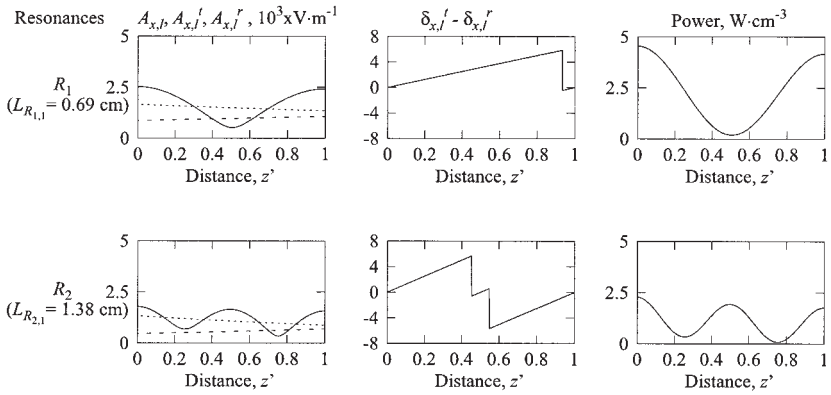

Figure 5. Amplitudes of electric field ($A_{x,l}$, $A_{x,l}^t$, $A_{x,l}^r$), phase difference ($\delta_{x,l}^t - \delta_{x,l}^r$), and power distributions for pure water slabs exposed to microwaves from the left face.

· · · , transmitted wave; – – – , reflected wave; — , stationary wave. f = 2450 MHz, I_{OL} = 3 W cm^{-2}, I_{OR} = 0. Spatial resonances in electric fields are qualitatively similar to that in oil. Because of greater dielectric loss of water, greater power absorption occurs following the similar trends in electric fields.

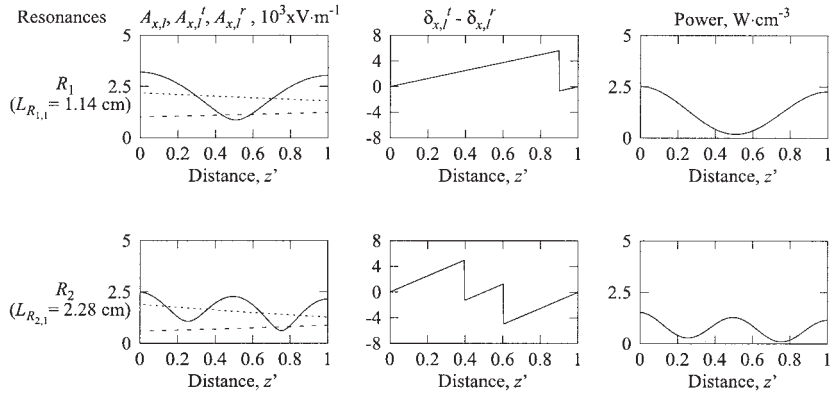

Figure 6. Amplitudes of electric field ($A_{x,l}$, $A_{x,l}^t$, $A_{x,l}^r$), phase difference ($\delta_{x,l}^t - \delta_{x,l}^r$), and power distributions for 50% o/w slabs exposed to microwaves from the left face.

$\cdots$, transmitted wave; – – –, reflected wave; —, stationary wave. f = 2450 MHz, I_{OL} = 3 W cm^{-2}, I_{OR} = 0. Qualitatively similar resonance features to that in water is observed. Power absorptions are lower than that in water.

waves at R_1 and R_2 are analyzed based on the influence of individual traveling waves attributed to transmission and reflection. We will carry out studies on the intensity of spatial resonance of absorbed power with spatial distributions of amplitudes ($A_{x,l}^t$; $A_{x,l}^r$; $A_{x,l}$) and difference between phase angles ($\delta_{x,l}$), where amplitudes and difference between phase angles are obtained from Eqs. 8 and 9. Figure 4 illustrates the amplitudes, difference between phase angles, and the MW power absorption for oil slabs. The two resonating length scales $L_{R_{1,1}}$ = 3.65 cm (N_w = 0.5) and $L_{R_{2,1}}$ = 7.3 cm (N_w = 1), corresponding to R_1 and R_2, respectively, are obtained from Figure 3. As seen in Figure 4, for both the sample thicknesses, the amplitude of the transmitted wave $A_{x,l}^t$ is greater than that of the reflected wave $A_{x,l}^r$. The amplitude of the stationary electric field has maxima at both faces for R_1, whereas for R_2 it has three maxima occurring at the center and both faces. Note that the phase difference between traveling waves, which is zero at the resonance, corresponds to a maximum in amplitude of the stationary wave. It is observed that for oil samples, the amplitude of the transmitted electric field varies within 3000–3800 V m^{-1}, whereas the reflected field is within 600–870 V m^{-1}. Note that the reflected electric field is 15–20% of transmitted field. For both thicknesses, the stationary electric field corresponds to very small spatial power absorptions ranging between 0.07 and 0.22 W cm^{-3} because of smaller dielectric loss of oil (see Table 1).

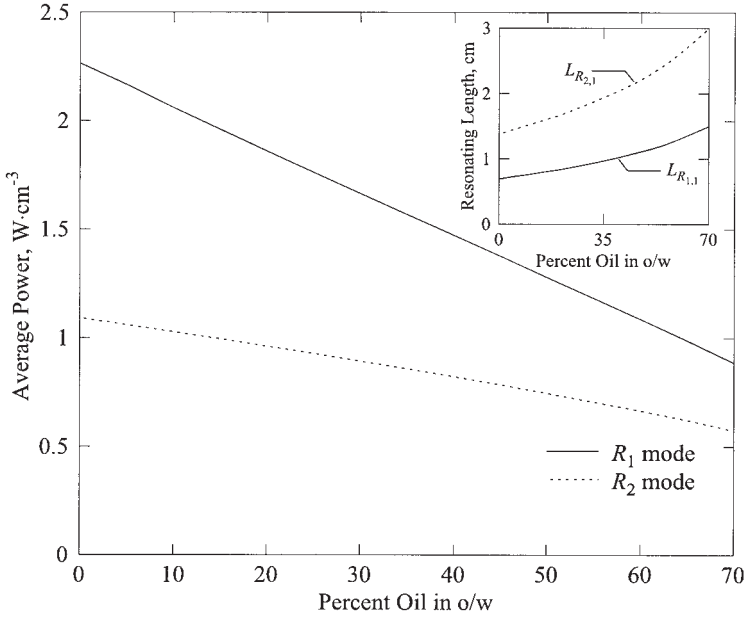

Figure 7. Average power (W cm^{-3}) vs. percent oil in o/w samples exposed to microwaves at one side for R_1 and R_2 modes.

f = 2450 MHz, I_{OL} = 3 W cm^{-2}, I_{OR} = 0. Average power is found to decrease with greater percentages of oil, and for greater percentages, the difference in average power between two resonance modes is smaller. Inset shows resonating lengths ($L_{R_{1,1}}$, $L_{R_{2,1}}$) vs percent oil in o/w.

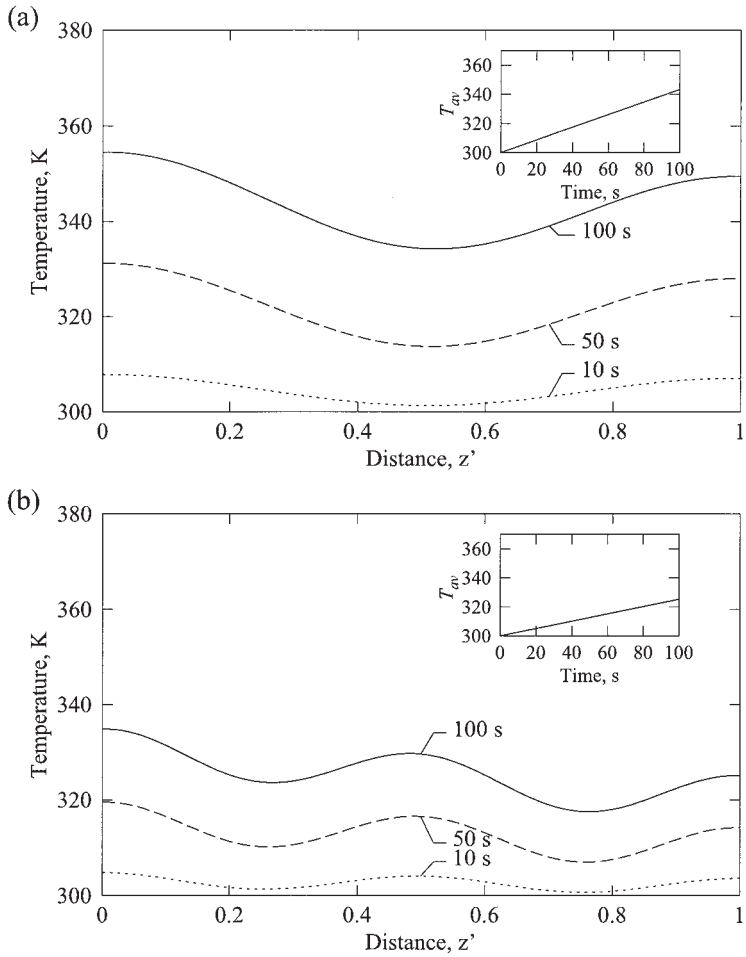

Figure 8. Temperature (K) vs. distance (cm) of 50% o/w samples at various time intervals during (a) R_1 mode with $L_{R_{1,1}}$ = 1.14 cm and (b) R_2 mode with $L_{R_{2,1}}$ = 2.28 cm.

f = 2450 MHz, I_{OL} = 3 W cm^{-2}, I_{OR} = 0. Temperature profiles show similar trend to power profiles as seen in Figure 6. Insets show average temperature vs. time, where a linear variation is observed for both resonance modes.

Figure 5 illustrates the spatial electric fields and power distributions for water samples. Similar to the oil sample, the resonance occurs at both faces for R_1 and three resonances at faces and center occur for R_2. For all cases, the amplitude of transmitted wave monotonically decreases with distance, whereas the amplitude of the reflected wave is of monotonically increasing order. Because of greater dielectric loss of water (see Table 1), the depth of penetration (D_p) within the water sample is 3.33 cm, whereas for the oil sample, D_p = 43.45 cm. Hence, the amplitude of the transmitted electric field within the water sample is within 800–1650 V m^{-1}, which is smaller than that in the oil sample and the amplitude of the reflected electric field within the water sample varies within 400–1000 V m^{-1}, during the R_1 and R_2 modes. Although the intensity of the stationary electric field within the oil sample is greater than that in the water sample, because of greater dielectric loss of water, the spatial and average power absorptions are greater in the water sample. The resonances R_1 and R_2 correspond to the length scales 0.69 and 1.38 cm, respectively, whereas for oil, the two consecutive resonances occur at 3.65 and 7.3 cm. Although for oil samples the greater thickness can be favored, water samples with smaller thickness correspond to much greater power absorption. These two contradicting features may play a critical role in determining power absorption in o/w and w/o samples with identical amounts of oil and water.

Figure 6 illustrates electric fields and power distributions for 50% o/w. Similar to oil and water samples, two spatial resonances for R_1 and three spatial resonances for R_2 are observed. A similar qualitative trend is also observed for the 50% w/o sample (figures are not shown). The stationary electric field distribution in the o/w sample varies within 800–3000 V m^{-1} during the R_1 mode. In contrast, the stationary field distribution in the w/o sample varies within 1200–3800 V m^{-1} at the similar resonance mode R_1. A similar trend is also observed at R_2. It is also observed that due to more wave penetration, the resonating lengths for both the R_1 and R_2 modes in the w/o sample are greater. Note that $L_{R_{1,1}}$ for the o/w sample is 1.14 cm and that for w/o sample is 1.58 cm.

Figure 7 illustrates average power vs. percent oil in the o/w sample. For both R_1 and R_2 modes, average power is a monotonically decreasing function with percent oil. Although the

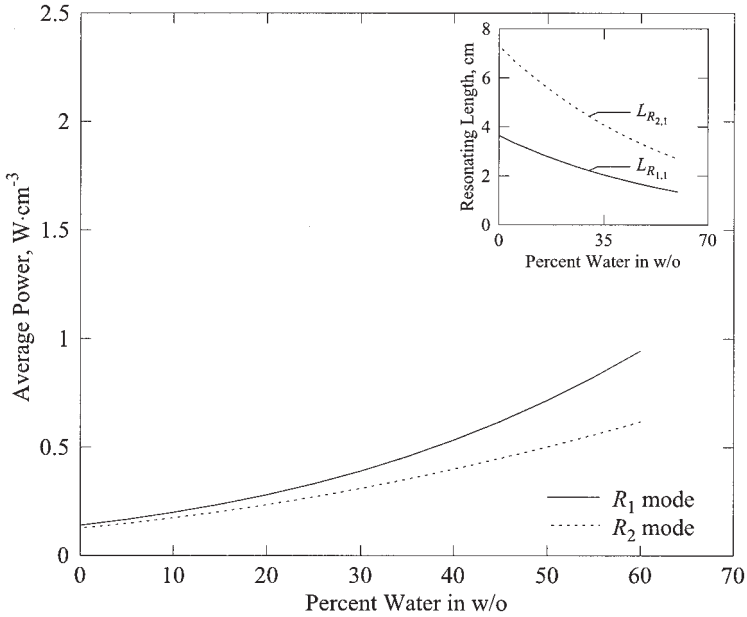

Figure 9. Average power (W cm^{-3}) vs. percent water in w/o samples exposed to microwaves at one side for R_1 and R_2 modes.

f = 2450 MHz, I_{OL} = 3 W cm^{-2}, I_{OR} = 0. Average power is found to increase with greater percentages of water, and for smaller percentages, the difference in average power between two resonance modes is smaller. Inset shows resonating lengths ($L_{R_{1,1}}$, $L_{R_{2,1}}$) vs. percent water.

penetration of waves within an o/w emulsion increases with increasing oil fraction, the effective dielectric loss decreases with oil fraction (as seen in Figure 2), resulting in a smaller average power distribution. In addition, the decrease in average power per unit volume is attributed to resonating lengths, $L_{R_{1,1}}$ and $L_{R_{2,1}}$, which increase with percentage oil fraction resulting from greater wavelengths corresponding to greater penetration. As stated earlier, $L_{R_{2,1}} = 2L_{R_{1,1}}$, and thus the average power absorption per unit volume in the R_1 mode is larger. However, for some o/w samples, heating with the R_2 resonant case may be advantageous to obtain a greater sample thickness to be processed at a faster rate. A detailed analysis on efficient use of MW power will be discussed later.

To investigate the thermal effects, the temperature distribution for o/w samples is shown in Figure 8. Figures 8a and 8b illustrate the temperature distributions of the 50% o/w sample for R_1 and R_2 modes, respectively, at various time intervals. Temperature distributions follow a trend similar to that of power distributions. The insets are average temperature vs. time distributions, where the average temperature varies linearly with time. For the R_1 mode the average temperature is 343 K at 100 s and the average temperature is 325.3 K during the R_2 mode, at the same time interval. During 100 s, the highest temperature at the left face is 354 K and the lowest temperature is around 334 K at the center for the R_1 mode. Because of spatial power resonances, the hot spots may occur within a sample. An on–off control of MW sources can be used to attain uniformity of temperature, as discussed in an earlier publication (Basak and Ayappa, 1997).

Figure 9 illustrates average power vs. percent water in the w/o sample. The average power is a monotonically increasing function with percent water resulting from greater effective dielectric loss as seen in Figure 2b. The inset of Figure 9b illustrates the resonating lengths vs. percent water. Because of less penetration for greater water percentages, the resonating lengths decrease with percent water for both the R_1 and R_2 modes. The temperature distribution for a 50% w/o sample shows a similar qualitative trend as that seen for the 50% o/w sample (figures are not shown for the 50% w/o sample). Similar to the o/w sample as seen in Figure 8, the average temperature varies linearly with time. For 50% w/o samples, it is found that during 100 s, the average temperature is 324.2 K at the R_1 mode, whereas at R_2 the average temperature is around 317 K, which is in contrast to the results for the 50% o/w sample, where the average temperature is higher at identical resonance conditions. In addition, for the 50% w/o sample, the variation in the average temperature between R_1 and R_2 is considerably lower, which is in contrast to that for the 50% o/w sample.

A representative case study on heating of the 50% o/w emulsion in the absence of resonance is shown in Figure 10. The thickness of the sample, $0.5L_{R_{1,1}} = 0.57$ cm, where a destructive interference occurs (see Figure 3). Figure 10a illustrates the spatial power distribution, which shows a maximum in power at the side not exposed to MWs. The power varies between 0.054 and 0.67 W cm^{-3}, which is much lower than that at the R_1 mode, as seen in Figure 6. During 100 s, the maximum increase in temperature is 14.5 K, as seen in Figure 10b. The average temperature (see inset of Figure 10b) is 312 K at 100 s, whereas at R_1 with $L_{R_{1,1}} = 1.14$ cm, the average temperature is 343 K during the same time interval. It is interesting to note that the significant influence of resonance in power absorption accelerates the heating process for a larger sample thickness corresponding to the R_1 mode. Similar fea-

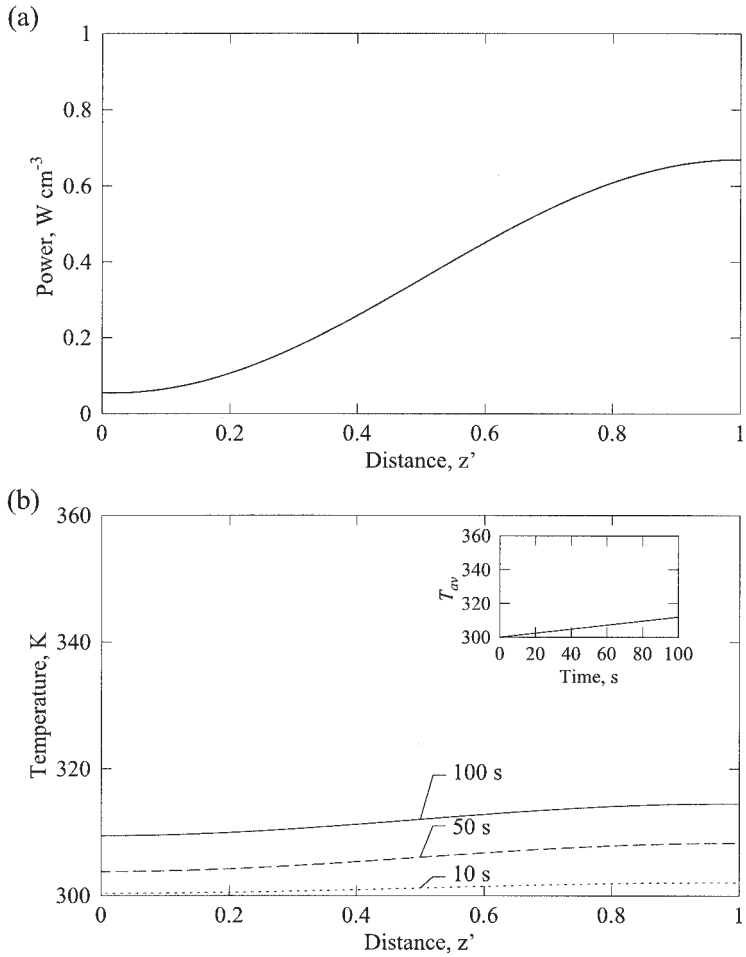

Figure 10. (a) Power (W cm^{-3}) vs. distance (cm) and (b) temperature (K) vs. distance (cm) for a 50% o/w slab in the absence of resonance.

The sample thickness is 0.57 cm. $f = 2450$ MHz, $I_{OL} = 3$ W cm^{-2}, $I_{OR} = 0$. The maximum in spatial power is observed at the face not exposed to microwaves. Overall, smaller spatial power deposition causes little heating rates throughout the sample.

tures can be observed for other sample thicknesses (figures are not shown).

To analyze the optimal MW power use, we analyze the heating effect with the lumped parameter heating model as

$$C_{eff}\frac{dT_{av}}{dt} = q_{av} \tag{36}$$

where T_{av} is the average temperature of a sample and q_{av} is the average power, defined in Eq. 14. Equation 36 provides an estimate of the average heating rate, whereas the heat loss is negligible, as $h = 2$ W m^{-2} K^{-1}. Note that, for a specific emulsion (o/w or w/o), the average heating rate is directly proportional to the average power q_{av} (see Eq. 36). The power usage by various resonance modes, either R_1 or R_2, can be analyzed with a power factor as

$$P_{f,1} = \frac{(q_{av,R_1})_1}{2(q_{av,R_2})_1} \tag{37}$$

Here $(q_{av,R_1})_1$ and $(q_{av,R_2})_1$ denote average power absorptions at $L_{R_{1,1}}$ and $L_{R_{2,1}}$, respectively. The outer suffix "1" denotes the one-side incidence only. Here, $P_{f,1} = 1$ denotes that either R_1 or R_2 is optimal, given that total power or heat absorption in both modes is identical; $P_{f,1} > 1$ corresponds to the greater power absorption at R_1; and $P_{f,1} < 1$ corresponds to the R_2 mode. Smaller $P_{f,1}$, corresponding to greater power absorption in the R_2 mode, represents the faster heating rate in the R_2 mode. Alternatively, the efficient heating strategy can be analyzed with the heating factor $h_{f,1}$, where

$$h_{f,1} = \frac{(\Delta\dot{T}_{av,R_1})_1}{2(\Delta\dot{T}_{av,R_2})_1} \tag{38}$$

Here $(\Delta\dot{T}_{av,R_1})_1$ and $(\Delta\dot{T}_{av,R_2})_1$ denote average heating rates (K s^{-1}) for $L_{R_{1,1}}$ and $L_{R_{2,1}}$, respectively. Here, $h_{f,1} = 1$ denotes that either R_1 or R_2 is optimal, given that total heat absorption in both the modes is identical; $h_{f,1} > 1$ corresponds to the greater heat absorption at R_1; and $h_{f,1} < 1$ corresponds to the

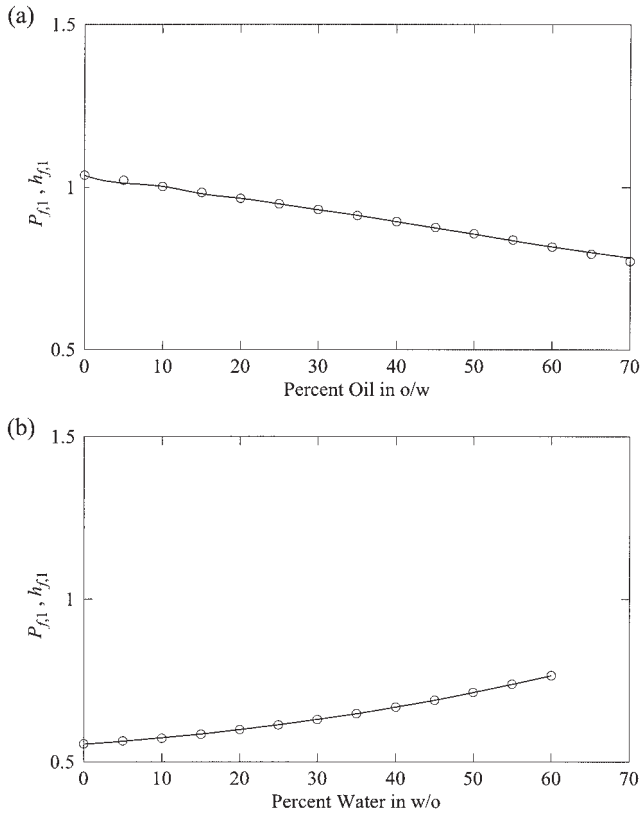

Figure 11. Power factor ($P_{f,1}$) and heating factor ($h_{f,1}$) profiles for (a) o/w and (b) w/o with various percent contents.

○, $(P_{f,1})$; —, $(h_{f,1})$. f = 2450 MHz, I_{OL} = 3 W cm^{-2}, I_{OR} = 0. For both emulsions, heating with R_2 mode is favored.

R_2 mode. In addition $h_{f,1} < 1$ denotes that an emulsion sample with greater resonating length $L_{R_{2,1}}$ exhibits a higher processing rate, which corresponds to time savings.

Figure 11a illustrates $P_{f,1}$ and $h_{f,1}$ vs. percent oil in the o/w sample where, except for lower oil percentages, both $P_{f,1}$ and $h_{f,1}$ are monotonically decaying functions with oil percentages. Both $P_{f,1}$ and $h_{f,1}$ are only slightly greater than 1 at lower oil percentages and factors are less than 1 at greater percentages, signifying that heating at the R_2 mode is advantageous for greater percentages of oil and operation at the R_2 mode corresponding to greater heating rate leads to less processing time. For w/o samples, both factors are monotonically increasing functions with percentage of water. The data are shown up to 60% w/o sample because beyond 60%, w/o emulsions are generally unstable. It is interesting to note that, for all percentages of water, the factors are much less than 1, signifying that heating at the R_2 mode for w/o samples is always advantageous. For all emulsions, the magnitudes of $P_{f,1}$ and $h_{f,1}$ are identical, thus justifying an analysis with the lumped parameter heating model as given in Eq. 36. The detailed energy balance equation is necessary to illustrate the spatial temperature gradients ascribed to strong spatial resonances. For specific cases, the spatial distribution is also necessary to identify the localized hot spots.

Both-sides incidence

Figure 12 illustrates average power vs. wavenumber (N_w) for oil, water, and oil–water emulsions for slabs with both sides exposed to MWs. The maxima in average power occur at N_w = 1 and N_w = 2, which correspond to R_1 and R_2, respectively, and the maxima occurring at fixed N_w are material invariant, as seen in Figure 12. Note that at N_w = 1, the secondary maximum at the R_2 mode occurs because of one-side incidence (see Figure 3). Let us denote the resonating length for the R_1 mode with both-sides incidence as $L_{R_{1,2}}$, which can be correlated with the one-side incidence case because $L_{R_{2,1}} = L_{R_{1,2}} = 0.5L_{R_{2,2}}$. The outer suffix "2" denotes the both-sides incidence. Based on various resonating lengths, the detailed analysis of power and temperature distributions in the presence of both-sides incidence cases play a critical role in deciding the efficient route to heating of oil–water emulsions.

The distribution of power within oil–water emulsions can be analyzed with electrical field distributions resulting from transmitted and reflected waves. The field and power distributions for the 50% o/w sample are illustrated in Figure 13. Because the sample is exposed at both sides, the transmitted and reflected fields are symmetric with each other, both for R_1 and R_2 modes. The stationary electric field has three maxima occurring at both faces and center during the R_1 mode. It is interesting to note that qualitatively similar field and power distributions occur at R_2 for one-side incidence, as seen in Figure 6. During the R_2 mode, multiple spatial resonances occur due to greater length, given that $L_{R_{2,2}} = 2L_{R_{1,2}}$ (Figure 13). The analysis was also carried out for 50% w/o samples, where similar features are also observed, except that stationary field and MW power distributions are smaller in the w/o sample, as discussed in the previous section (figures are not shown).

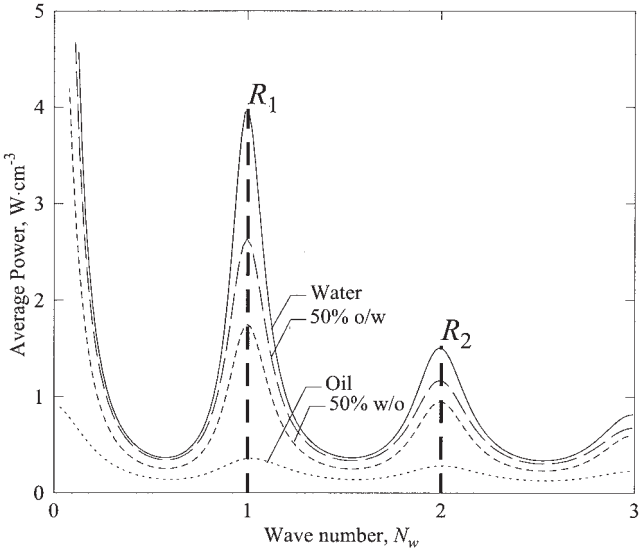

Figure 12. Average power (W cm^{-3}) vs. wavenumber (N_w) for water, oil, 50% o/w, and 50% w/o slabs exposed to microwaves at both sides.

f = 2450 MHz, $I_{OL} = I_{OR}$ = 3 W cm^{-2}. The primary maximum in average power occurs at N_w = 1, corresponding to R_1 resonance mode, whereas a secondary resonance mode R_2 occurs at N_w = 2, irrespective of any materials.

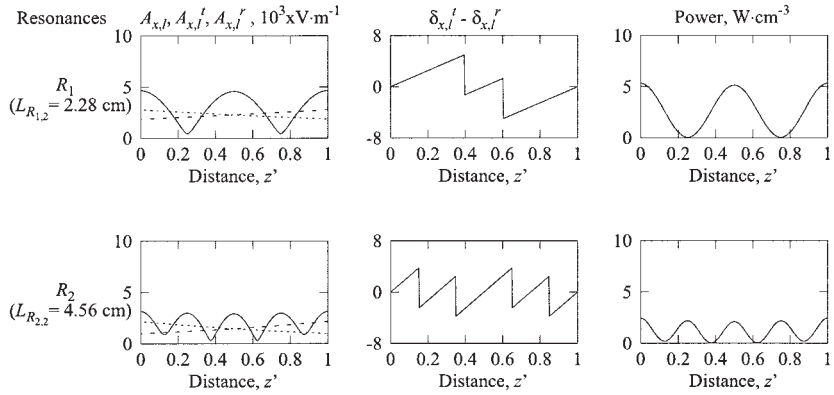

Figure 13. Amplitudes of electric field ($A_{x,l}$, $A_{x,l}^t$, $A_{x,l}^r$), phase difference ($\delta_{x,l}^t - \delta_{x,l}^r$), and power distributions for 50% o/w slabs exposed to microwaves from the left face.

· · ·, transmitted wave; – – –, reflected wave; —, stationary wave. f = 2450 MHz, $I_{OL} = I_{OR}$ = 3 W cm^{-2}. Multiple resonance peaks with smaller intensities for spatial power absorptions are observed during R_2 mode.

Figure 14 illustrates the temperature distributions for 50% o/w samples. Similar to one-side incidence cases, the temperature distribution follows similar power distributions. At 60 s, the average temperature is around 353 K during the R_1 mode, which is in contrast to 326 K attributed to one-side incidence during the R_2 mode. Note that the total power incidence is

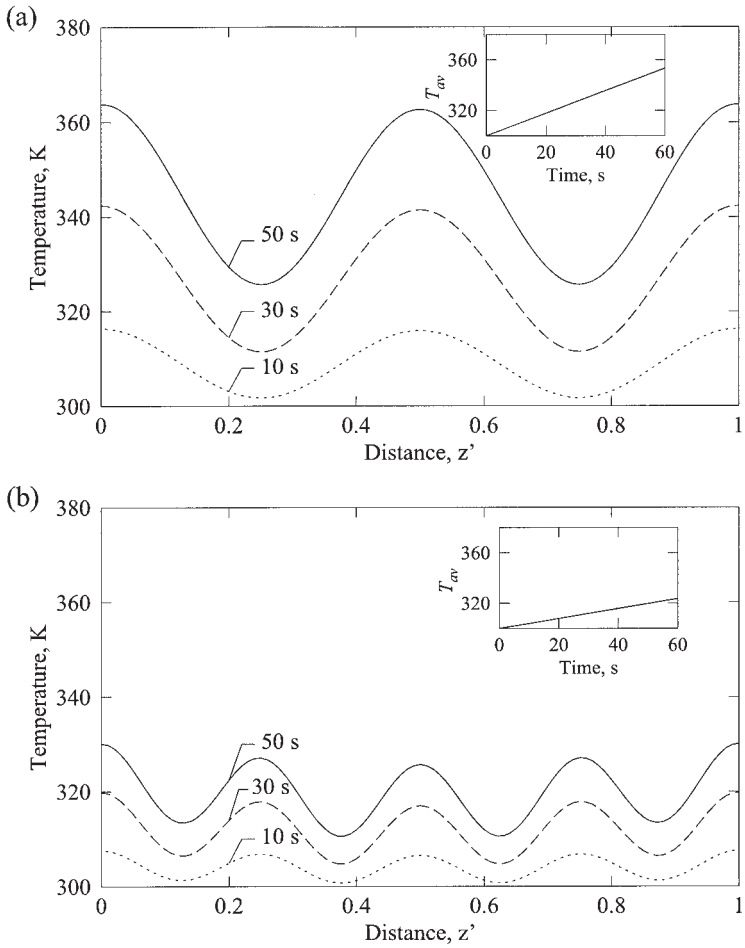

Figure 14. Temperature (K) vs. distance (cm) of 50% o/w samples at various time intervals during (a) R_1 mode with $L_{R_{1,2}}$ = 2.28 cm and (b) R_2 mode with $L_{R_{2,2}}$ = 4.56 cm.

f = 2450 MHz, $I_{OL} = I_{OR}$ = 3 W cm^{-2}. Temperature profiles show similar trend to power profiles as seen in Figure 13. Insets show average temperature vs. time, where a linear variation is observed for both resonance modes.

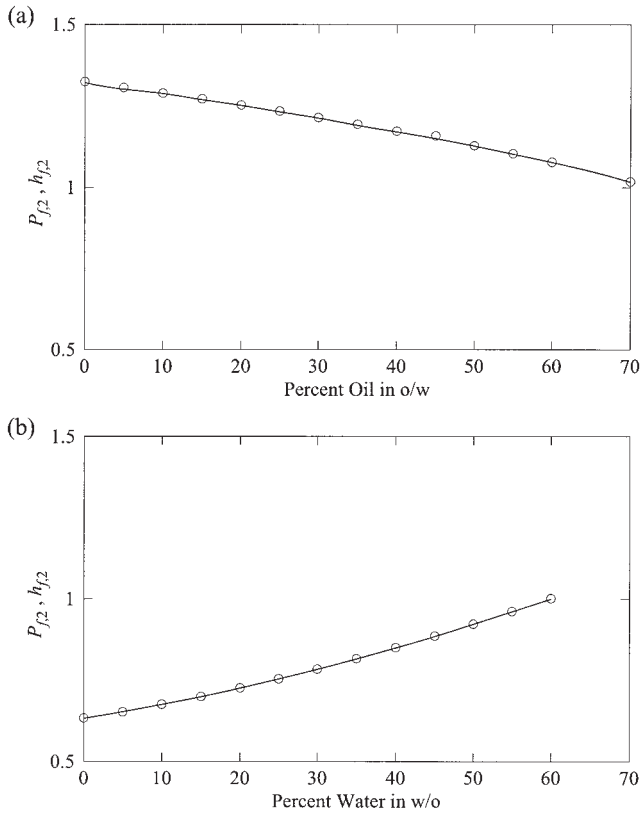

Figure 15. Power factor ($P_{f,2}$) and heating factor ($h_{f,2}$) profiles for (a) o/w and (b) w/o with various percent contents.

○, ($P_{f,2}$); —, ($h_{f,2}$). f = 2450 MHz, $I_{OL} = I_{OR}$ = 3 W cm^{-2}. For o/w emulsion, R_1 mode is favored, whereas R_2 mode is efficient for w/o emulsion. Note that, during one-side incidence, R_2 mode is always the favorable mode for both o/w and w/o emulsions.

doubled at the both-sides incidence case with $L_{R_{1,2}} = L_{R_{2,1}}$. During the R_2 mode, the spatial variation of temperature is smaller than that at the R_1 mode. Similar to the one-side incidence case, the 50% w/o sample exhibits smaller heating effects than those of the 50% o/w sample, as discussed in the previous section.

The optimal power use for both-sides incidences can be analyzed by use of a lumped parameter heating model as discussed with respect to Eq. 36. Similar to one-side incidence cases, the power factor for both-sides incidence cases $P_{f,2}$ is represented as

$$P_{f,2} = \frac{(q_{av,R_1})_2}{2(q_{av,R_2})_2} \tag{39}$$

and the heating factor

$$h_{f,2} = \frac{(\Delta \dot{T}_{av,R_1})_2}{2(\Delta \dot{T}_{av,R_2})_2} \tag{40}$$

The outer suffix "2" represents the both-sides incidence case. Figures 15a and 15b represent distributions of the power and heating factors for o/w and w/o samples, respectively. For o/w samples, both factors linearly decrease with percent oil, similar to the one-side incidence case as seen in Figure 11a. For both-sides incidence cases, the factors vary between 1.3 and 1 and, therefore, the R_1 mode operation is optimal, whereas for one-side incidence cases, the R_2 mode operation is optimal. For w/o samples, the factors varying between 0.6 and 1 signify that the R_2 mode is favorable. A similar situation is also observed for one-side incidence cases, as seen in Figure 11b.

Efficient power use: one side vs. both sides

Finally, we illustrate the efficient use of power with the effective power factor for o/w and w/o samples. Here, the definition of effective factors for the o/w sample will differ from that for the w/o sample. The definitions of effective factors are based on the efficient resonance modes (R_1 or R_2) corresponding to one-side incidence and both-sides incidence cases. For o/w samples, the R_2 mode of heating for one-side cases will be contrasted with the R_1 mode of heating for both-sides incidence cases. Therefore, the effective power factor ($P_{f_{o/w}}$) and the effective heating factor ($h_{f_{o/w}}$) for the o/w samples are, respectively

$$P_{f_{o/w}} = \frac{(q_{av,R_2})_1}{0.5(q_{av,R_1})_2} \tag{41}$$

and

$$h_{f_{o/w}} = \frac{(\Delta \dot{T}_{av,R_2})_1}{0.5(\Delta \dot{T}_{av,R_1})_2} \tag{42}$$

The outer suffixes "1" and "2" correspond to the one-side incidence case and both-sides incidence cases, respectively. Figure 16a illustrates the effective power and heating factors vs. percent oil for o/w samples. For all the percent oil contents, both factors are found to vary within 0.55–0.58, which indicates that the both-sides incidence with the R_1 mode is efficient. In addition, the factors around 0.55 correspond to greater heating rates with time savings. The inset denotes the effective processing length, $L_{R_{1,2}}$ vs. percent oil, which indicate that the processing lengths for o/w samples vary within 1.38 to 3 cm.

The effective factors for w/o samples are defined as

$$P_{f_{w/o}} = \frac{(q_{av,R_2})_1}{(q_{av,R_2})_2} \tag{43}$$

and

$$h_{f_{w/o}} = \frac{(\Delta \dot{T}_{av,R_2})_1}{(\Delta \dot{T}_{av,R_2})_2} \tag{44}$$

Figure 16b illustrates variation in effective power and heating factors vs. percent water for w/o samples. The factors vary between 0.45 and 0.57 for various fractions of water that correspond to the both-sides incidence case. The inset shows the effective processing length, $L_{R_{2,2}}$ vs. percent water. Note that the processing lengths vary from 14.6 to 5.4 cm, which are

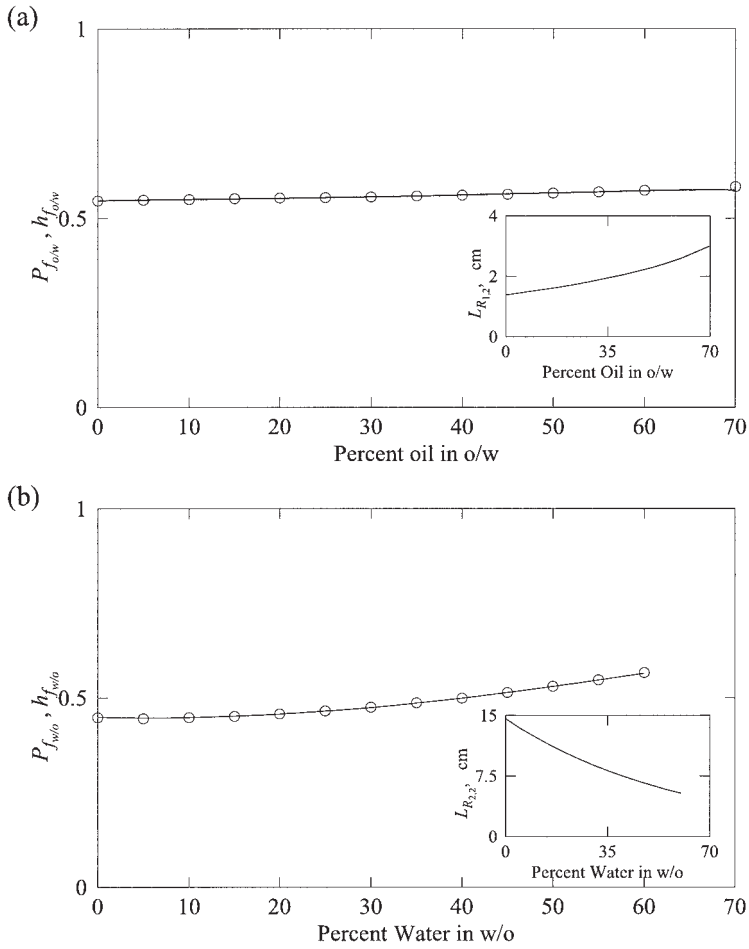

Figure 16. (a) Power factor ($P_{f,o/w}$) and heating factor ($h_{f,o/w}$) profiles for (a) o/w and (b) power factor ($P_{f,w/o}$) and heating factor ($h_{f,w/o}$) profiles for w/o with various percent contents.

○, power factor; —, heating factor. The parameters on MW incidence are as stated in previous figures. The both-sides incidence is the efficient mode to heat both o/w and w/o emulsions. Insets show the resonating lengths corresponding to efficient resonance mode during both-sides incidence.

greater than the effective processing lengths for o/w samples. However, the average heating rate for o/w samples is greater, as discussed in earlier sections.

For o/w and w/o emulsions, both-sides incidences are preferred because of their greater heating rates leading to a faster processing of sample. It may be interesting to analyze the fractional power use for one-side and both-sides incidence cases, where the fractional power use is

$$P_u = \frac{(q_{av,R_i})_j L_{R_{i,j}}}{jI_0} \tag{45}$$

where j denotes either one-side ($j = 1$) or both-sides incidence ($j = 2$) cases, R_i is the efficient resonance mode corresponding to $j = 1$ or $j = 2$, and $I_0 = 3$ W cm^{-2} is the incident microwave radiation intensity. Therefore, $P_u = 1$ signifies that MW incident radiation is completely used to produce heat within the samples and $P_u < 1$ denotes that some fraction of MW energy is lost within samples as a result of destructive interferences. Figure 17a represents P_u vs. percent oil in the o/w sample for both cases, where we find the fractional power use is greater in both-sides cases in the R_1 mode. Note that for the one-side case, around 50% of incident MW energy is used by the samples for heating, whereas samples use 90–100% MW energy for both-sides cases. For 50% o/w samples, $P_u > 1$ corresponds to a greater effect of resonances within the sample. Figure 17b illustrates P_u vs. percent water in the w/o sample, where P_u varies within 0.68–1 during both-sides incidence. Although at low percentages of water MW energy is lost mostly because of reflection, at higher water fractions, MW energy is used up to 100%. The greater resonating effect leading to $P_u > 1$ is also observed at around 50% w/o samples. It is interesting to note that for both o/w and w/o samples, the fractional power use P_u increases with the fraction of the dispersed phase. This analysis also indicates that for 45–50% o/w or w/o samples an enhanced heating rate at both-sides incidence also corresponds to maximum MW power use.

Conclusion

We have carried out extensive studies to investigate the influence of MW power resonances on heating of oil–water emulsions, where the sample is either incident with MWs at

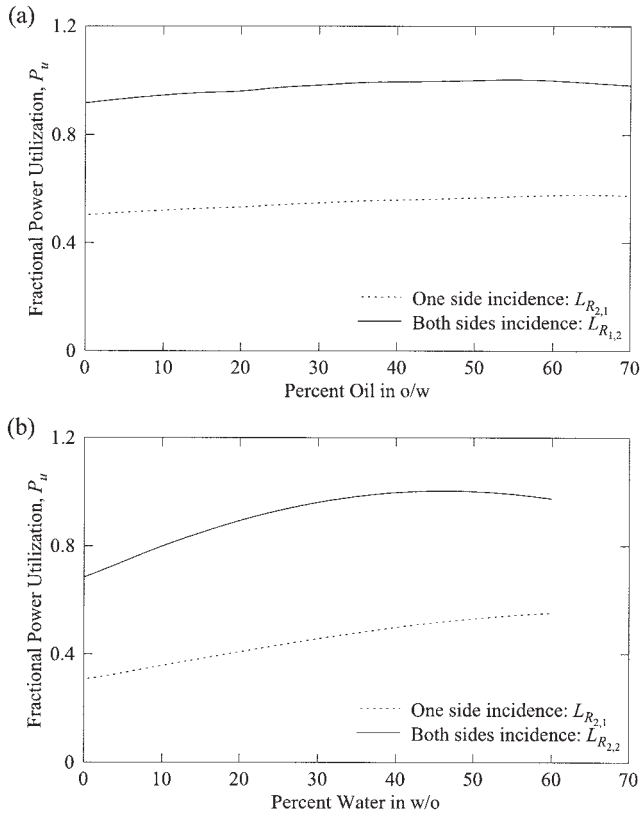

Figure 17. Fractional power utilization, P_u vs. (a) percent oil in o/w samples and (b) percent water in w/o samples.

The parameters on MW incidence are as stated in previous figures. During both-sides incidence, almost 80–100% of incident microwave power has been utilized.

one side or both sides. The power absorption within an emulsion is strongly dependent on the nature of the continuous medium based on the models for effective dielectric properties (Erle et al., 2000). The maximum in average power corresponds to various resonance modes occurring at fixed wavenumbers, where the wavenumber is defined as the ratio of sample thickness to the wavelength of MWs within the sample. For a fixed wavenumber, materials such as oil, water, and various emulsions will correspond to various resonating lengths. Our detailed analysis involves identification of particular resonance modes, processing lengths, heating strategy, and MW power savings for specific o/w or w/o emulsions.

A detailed analysis on MW power absorption has been illustrated with the distributions of transmitted and reflected waves for oil, water, and various emulsions. For oil samples, the reflected electric field intensity is 15–20% of transmitted field, whereas for water samples the transmitted and reflected fields are within a similar order of magnitude during both R_1 and R_2 modes. Although the total electric field for the oil sample is larger than that for water sample, attributed to greater dielectric loss of water, greater power absorption is observed for the water sample. The qualitative features of electric fields and power absorptions within the 50% o/w sample and 50% w/o samples are identical, but greater spatial electric fields and power absorption are observed for the o/w samples. The difference in power absorption for the o/w and w/o samples with identical oil and water fractions is investigated further to examine the efficient heating strategies for o/w and w/o samples.

The heating characteristics within a material are modeled using the energy balance equation and Maxwell's equations for MW power. The temperature distributions are seen to be qualitatively similar with the power distributions. However, the detailed energy balance may be useful to identify the hot spots for some specific cases. A lumped parameter model for heating indicates that average power is directly proportional to the average heating rate. The average power absorption is found to decrease with percent oil for o/w samples, whereas for w/o samples, the average power increases with percent water. The efficient resonance mode corresponding to greater heating rates, at either the R_1 or the R_2 mode, has been examined both for o/w and w/o samples with various fractions of dispersed phases. It has been observed that for one-side MW incidence, the R_2 mode is favored both for o/w and w/o emulsions, whereas for both-sides incidences, the R_1 mode for o/w and the R_2 mode for w/o emulsions are favored. The heating rates for one-side incidence and both sides incidence cases have also been contrasted, and for all oil–water emulsions, both-sides incidence cases were found to be efficient for heating the emulsions. For fixed incident MW intensities, o/w and w/o samples correspond to maximum power use during both-sides MW incidence and both 50% o/w and w/o samples exhibit 100% MW power use. Although the MW power expenditure is less for the one-side incidence, power wastage is significant as a result of destructive interference within the medium, whereas greater MW expenditure during both sides minimizes the destructive interference.

The present analysis provide guidelines to efficiently heat oil–water emulsions. Although the processing sample thicknesses or resonating lengths are small, the heating rate is a very strong function of sample length scales, orientation of MW incidences, and nature of emulsion, attributed to strong resonating effects. In reality, during custom oven experiments that may operate with uniform plane wave, the emulsion heating would be guided by the fact that heating of particular emulsions depends on the particular sample dimensions for a maximum heating effect. Therefore, the results on efficient heating of emulsions of a 1-D slab are particularly useful for emulsion processing, and an extension of the present theoretical analysis for emulsions of 2-D cylinders would be an important contribution in future research. Household microwave ovens operate under multidirectional MW fields that may weaken the effective field within the sample; however, the strong size-dependent and counterintuitive heating, based on the nature of emulsions, may be observed for samples having small dimensions.

Literature Cited

Ayappa, K. G., "Resonant Microwave Power Absorption in Slabs," *J. Microwave Power & Electromagn. Energy,* **34**, 33 (1999).

Ayappa, K. G., H. T. Davis, S. A. Barringer, and E. A. Davis, "Resonant Microwave Power Absorption in Slabs and Cylinders," *AIChE J.,* **43**, 615 (1997).

Ayappa, K. G., H. T. Davis, G. Crapiste, E. A. Davis, and J. Gordon, "Microwave Heating: An Evaluation of Power Formulations," *Chem. Eng. Sci.,* **46**, 1005 (1991).

Ayappa, K. G., H. T. Davis, E. A. Davis, and J. Gordon, "Two-Dimensional Finite Element Analysis of Microwave Heating," *AIChE J.,* **38**, 1577 (1992).

Barringer, S. A., K. G. Ayappa, E. A. Davis, H. T. Davis, and J. Gordon, "Power Absorption During Microwave Heating of Emulsions and Layered Systems," *J. Food Sci.,* **60**, 1132 (1995).
Barringer, S. A., E. A. Davis, J. Gordon, K. G. Ayappa, and H. T. Davis, "Effect of Sample-Size on the Microwave-Heating Rate—Oil vs. Water," *AIChE J.,* **40**, 1433 (1994).
Basak, T., "Analysis of Resonances During Microwave Thawing of Slabs," *Int. J. Heat & Mass Transfer,* **46**, 4279 (2003).
Basak, T., and K. G. Ayappa, "Analysis of Microwave Thawing of Slabs with Effective Heat Capacity Method," *AIChE J.,* **43**(7), 1662 (1997).
Basak, T., and K. G. Ayappa, "Influence of Internal Convection During Microwave Thawing of Cylinders," *AIChE J.,* **47**, 835 (2001).
Basak, T., and K. G. Ayappa, "Role of Length Scales on Microwave Thawing Dynamics in 2D Cylinders," *Int. J. Heat & Mass Transfer,* **45**, 4543 (2002).
Chan, C. C., and Y. C. Chen, "Demulsification of W/O Emulsions by Microwave Radiation," *Sep. Sci. Technol.,* **37**, 3407 (2002).
Chatterjee, A., T. Basak, and K. G. Ayappa, "Analysis of Microwave Sintering of Ceramics," *AIChE J.,* **44**, 2302 (1998).
Erle, U., M. Regier, C. Persch, and H. Schubert, "Dielectric Properties of Emulsions and Suspensions: Mixture Equations and Measurement Comparisons," *J. Microwave Power & Electromagn. Energy,* **35**, 185 (2000).
Fang, C. S., and P. M. C. Lai, "Microwave Heating and Separation of Water-in-Oil Emulsions," *J. Microwave Power,* **30**, 46 (1995).
Fricke, H., "The Complex Conductivity of a Suspension of Stratified Particles of Spherical or Cylindrical Form," *J. Phys. Chem.,* **59**, 168 (1955).
Fu, W., and A. Metaxes, "A Mathematical Derivation of Power Penetration Depth for Thin Lossy Materials," *J. Microwave Power & Electromagn. Energy,* **27**, 217 (1992).
Lichtenecker, K., and I. Rother, "Die Herleitung des Logarithmischen Mischungsgestezes aus Allegemeinen Prinzipien der Stationären Strömung," *Physikalische Zeitschrift,* **32**, 255 (1931).
Massoudi, H., C. H. Durney, P. W. Barber, and M. F. Iskander, "Electromagnetic Absorption in Multilayered Cylinder Models of Man," *IEEE Trans. Microwave Theory & Techniques,* **27**, 825 (1979).
Ohlsson, T., and P. O. Risman, "Temperature Distribution of Microwave Heating-Spheres and Cylinders," *J. Microwave Power,* **13**, 303 (1978).
Pescheck, P., W. H. Atwell, M. Krawjecki, and G. Anderson, U.S. Patent No. 5 140 121 (1992).
Ratanadecho, P., K. Aoki, and M. Akahori, "A Numerical and Experimental Investigation of the Modeling of Microwave Heating for Liquid Layers Using a Rectangular Wave Guide (Effects of Natural Convection and Dielectric Properties)," *Appl. Math Modeling,* **26**, 449 (2002).
Weil, C. M., "Absorption Characteristics of Multilayered Sphere Models Exposed to UHF/Microwave Radiation," *IEEE Trans. Biomed. Eng.,* **BME-22**, 468 (1975).

Manuscript received Nov. 2, 2003, and revision received Jan. 28, 2004.